Journal of Geophysical Research: Planets

Supporting Information for

Spatial and Temporal Variation of Mars South Polar Ice Composition from Spectral Endmember Classification of CRISM Mapping Data

S. F. A. Cartwright[1,2], W. M. Calvin[3], K. D. Seelos[2], and F. P. Seelos[2]

[1]Department of Geological Sciences, Laboratory for Atmospheric and Space Physics, University of Colorado, Boulder, CO, USA, [2]Johns Hopkins University Applied Physics Laboratory, Laurel, MD, USA, [3]Department of Geological Sciences and Engineering, University of Nevada, Reno, NV, USA

Contents of this file

Introduction

The text description and three figures included in this file provide additional context for the process of deriving the final endmembers presented in the main text. Specifically, they detail how the original targeted data endmember set from Cartwright et al. (2022)(Fig. S1a) was subsampled to mapping data wavelengths (Fig. S1b), how those endmembers were combined to make 13 reference spectra (Fig. S2a), and how candidate endmembers from the mapping dataset were assigned to those reference spectra (Fig. S2b). A comparison of spectral feature strength between mapping and targeted endmembers is also presented (Fig. S3).

Text S1.

As described in Section 3 of the main text, south polar CRISM mapping data were processed with *k*-means clustering and random forest classification to extract a set of 30 candidate spectral endmembers. These endmembers characterize the diversity of spectral variation present in the mapping dataset. In Cartwright et al. (2022), we used similar processing techniques to derive a set of 21 spectral endmembers that characterize the diversity of spectral variation present in the CRISM targeted dataset. To compare the results of these two investigations, it was necessary to assign each of the

new candidate mapping endmembers to an appropriate endmember identified with targeted data. This process is outlined in Figure 2 in the main text and elaborated below.

To enable a more direct comparison of the spectral structures captured in both datasets, we first downsampled the original 21 targeted endmembers (Fig. S1a) from their original 438 shortwave-infrared channels to the set of 55 sampled in mapping data (Fig. S1b). However, this process removed or subdued spectral differences present in the suite of 21 targeted endmembers, meaning that some of the downsampled spectra were no longer meaningfully separable. We therefore found it necessary to combine some endmembers in a process illustrated in Figure S2a. This combination process produced a collection of 13 reference spectra to which the 30 candidate mapping data endmembers could be compared.

The 13 reference spectra still capture the range of spectral diversity present in the original targeted endmember set, but without the resolution needed to separate some pairings within compositional gradations. In general, we found that the endpoints of the gradations remained distinct (e.g., Dc1 and Dc3), but that intermediate endmembers (e.g., Dc2) could be combined with one endpoint or the other.

To assign candidate endmembers, we visually compared the spectra of a given candidate to all 13 reference spectra and determined which pairing had the most similar spectral structure (i.e., strengths and combinations of CO_2 and H_2O ice absorptions). Where this spectral assignment was ambiguous, we looked at the endmember distribution in classified mapping data mosaics. The final endmember assignments for each of the 30 candidates is visualized in Figure S2b.

Of the 13 reference spectra, 12 of them were found to be present in the mapping data results from random forest classification. Only one reference endmember (Cw1) was not found to have an equivalent in the mapping dataset; see the main text for possible explanations of this absence. Additionally, some CO_2 ice-rich endmembers and three apparent error modes (see Fig. S2b) were difficult to assign based on spectral features alone so they were isolated in mosaics and assigned based on spatial correlation with other endmembers.

The result of this process was a reassignment scheme used to reclassify the random forest results. This produced a final set of 12 mapping data endmembers and a collection of endmember-classified maps directly linked to the compositional framework described in Cartwright et al. (2022).

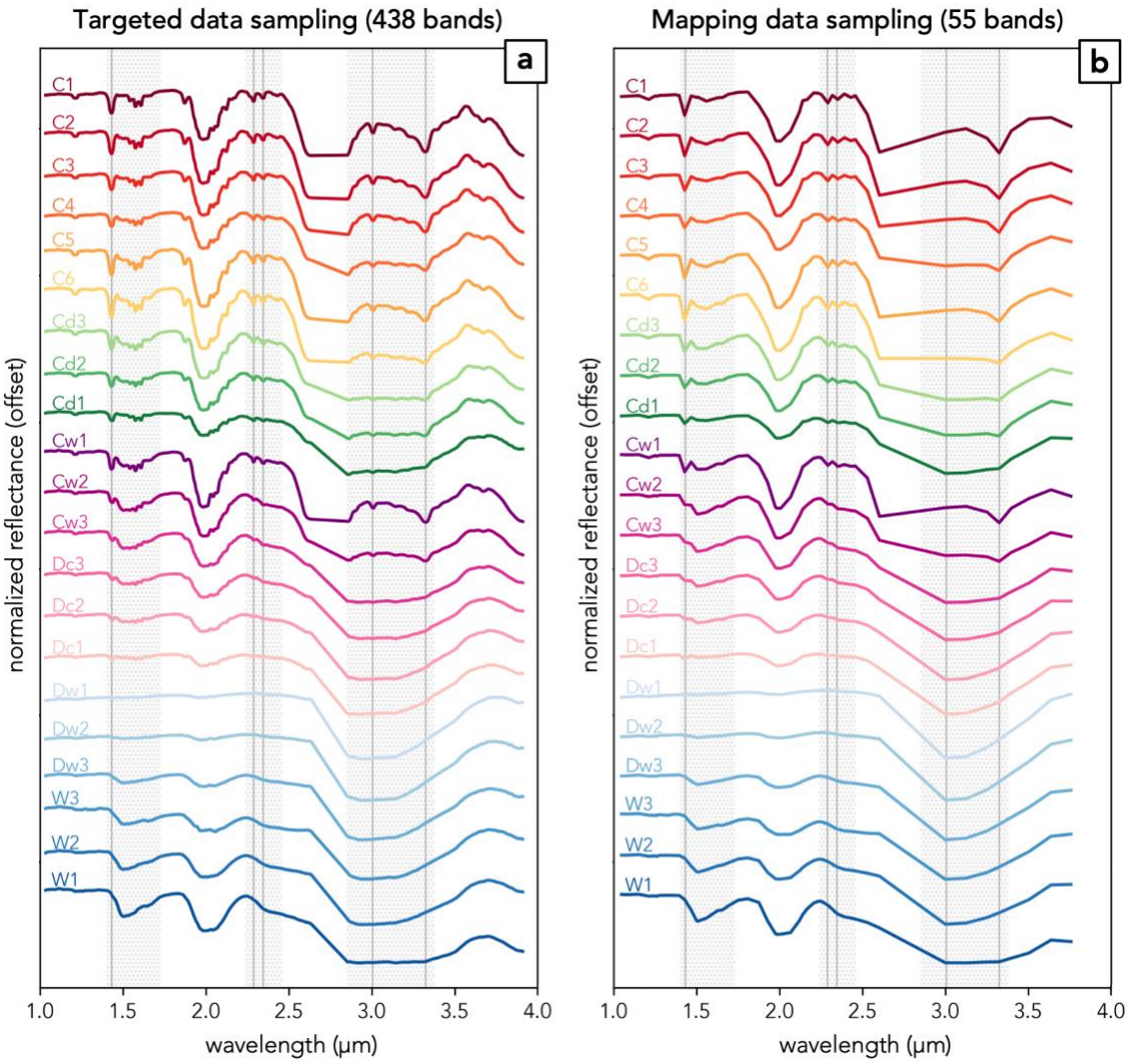

Figure S1. (a) The endmember set presented in Cartwright et al. (2022) derived from CRISM targeted data at the full spectral resolution of 438 SWIR channels. (b) The same endmembers when subsampled to the 55 spectral channels present in MSP and MSW data. Due to the removal of consistently suspect spectral channels, the actual band counts for targeted and mapping data used in these studies is 404 and 51, respectively. In both plots, vertical lines indicate narrow absorption features associated with CO_2 ice while hatched regions mark the bounds of broader absorptions associated with H_2O ice.

Note that even weaker expressions of each of these key features at full resolution are still visible in the subsampled set. A major exception is the region around 2.9–3.4 μm.

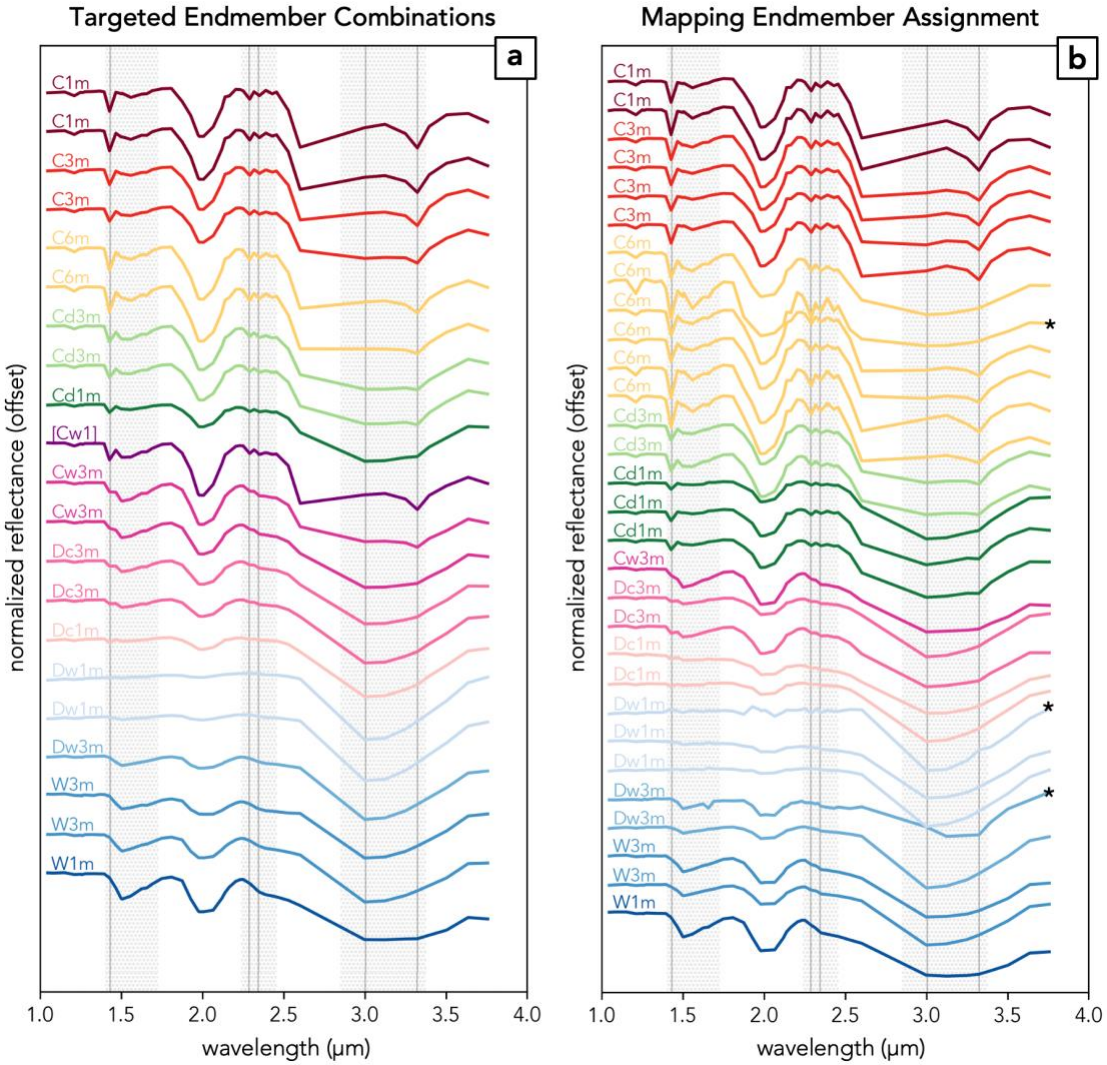

Figure S2. (a) The subsampled endmembers from Cartwright et al. (2022) colored and labeled according to how they were combined to create the 13 reference endmembers. Note the broad similarities in feature combinations and strengths between pairs that share the same color. Endmember Cw1 is also included here, though it was not found to be comparable to any of the candidate endmembers identified in CRISM mapping data. (b) The 30 candidate endmembers identified in mapping data colored and labeled according to which of the final 12 endmembers they were assigned to. Asterisks at the far right mark three endmembers associated with apparent error modes, which are expressed as noisy or otherwise unusually shaped spectra; these were assigned to an endmember based on spatial association with other endmembers in classified mosaics. Note that the six endmembers reclassified to C6m have consistently strong ~1.6 μm features that distinguish them from endmembers reclassified to C1m and C3m, but that

there are subtle differences in 1.5 μm feature strength that reflect the amount of water ice present.

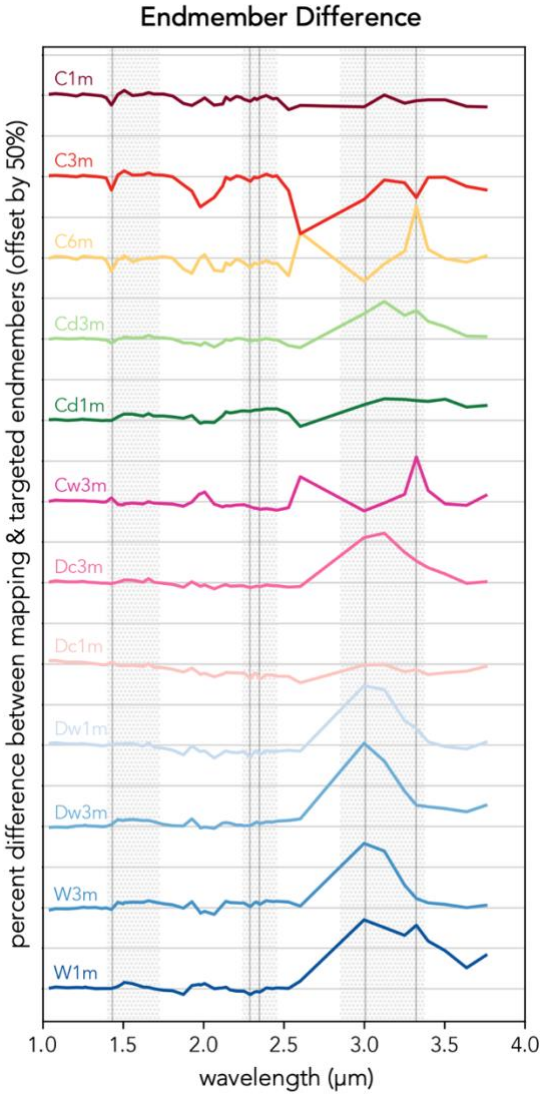

Figure S3. Plot of the percent difference between the mapping data endmembers shown in Figure 3 in the main text and the corresponding spectra for subsampled targeted data endmembers. Spectra are offset in 50% intervals and horizonal lines mark each 25% interval. Vertical lines mark narrow CO_2 ice features while hatched regions mark broad H_2O ice absorptions. Features that appear to jut above the continuum represent places where spectral features are weaker in mapping data while those that point downward indicate stronger features in mapping data. Pronounced differences at long wavelengths can be attributed to the CRISM filter boundary and suspect radiometry. In general, mapping data endmembers have stronger CO_2 ice features in CO_2 ice-dominated spectra, but weaker H_2O ice features in H_2O ice-dominated spectra compared to the corresponding targeted endmember.